



Liquefaction-induced damage to buried structures during different seismic events

Ahmed O. Mahmoud¹, Mourad Karray², Mohamed Chekired³, Mahmoud N. Hussien⁴, Carole Bessette³,
Livius Jinga³

¹ Ph.D. Student, Department of Civil and Building Engineering, University of Sherbrooke - Sherbrooke, QC, Canada.

² Professor, Department of Civil and Building Engineering, University of Sherbrooke - Sherbrooke, QC, Canada.

³ Hydro-Québec, Montréal, QC, Canada.

⁴ Associate Professor, Department of Civil Engineering, Faculty of Engineering, Assiut University, Assiut, Egypt.

ABSTRACT

Soil liquefaction beneath and around underground structures developed due to the increase of the pore water pressure during a seismic event constitutes one of the most important damaging reasons of these structures. The built up of pore water pressure during strong earthquakes would also lead to a significant uplift of the buried structure which has a direct impact on its functionality. This complex soil-structure interaction problem always poses challenges to practitioner and design engineers as it requires a rigors consideration of geometrical and material modelling aspects of the problem as well as the characteristics of earthquakes used in the computations. In this paper, the seismic behavior of access underground structures embedded in sandy deposits was studied using the three-dimensional (3D) finite differences (FD) program FLAC^{3D}. The energy-based approach that can simulate cyclic liquefaction by estimate built-up pore water pressure was incorporated in the program to model the behavior of the sandy deposit. Liner Structural Elements were used to model the underground structure. Numerical modeling has been carried out to investigate the structural and the soil performances under three different historical earthquakes with similar durations but different frequency contents. The PGAs of these earthquakes were modified to 0.5, 1.0, and 1.5 g to study the amplitude factors. It is found that the effect of frequency content on the structure and the soil behavior is not less important than the amplitude factor effect and in some situations the multiplication of the earthquake frequency leads to more alter in the excess pore water pressure of the soil and consequently the structural internal forces than it would do the earthquake amplitude.

Keywords: underground structure; finite difference; liquefaction; frequency content; excess pore water pressure; internal forces.

INTRODUCTION

Canada in general and Quebec in particular face several types of problems and destructions as a result of the transfer of electricity to homes above the ground through overhead lines. Much of the destruction has been recorded throughout history because of the destruction of storms to the ground power lines. In 1998, about 1,000 steel electrical pylons and 35,000 wooden utility poles were crushed and crumpled due to freezing rain occurred in Quebec, further damaging power supply and hampering the return of electricity [1]. To avoid this type of problems, it is now a common practice to transfer the electricity inside underground lines which is passing through access underground structures. In fact, the underground structures improve the landscape and protect electrical equipment from bad weather. In Quebec, during the last few decades, 11% of the overhead lines had been changed to below ground lines over the province. with the installation of more than 30,000 access underground structures. The construction of such lines and structures is very expensive however replacing these structures because of getting out service after earthquake occurring is more expensive [2]. For this reason, it is of importance to properly design these lines and structures against potential earthquakes.

There are several reports on devastations of underground structures caused by seismic loadings. In 1995 through Kobe earthquake, about 100 m of National Highway above the Daikai Station had settled by up to 3 to 4 m, over a width of 30 m which leads to damage to the subway system in Kobe city [3]. Substantial damage to buildings and underground structures have been reported after the 6.3 magnitude earthquake and its aftershocks in the Christchurch's central city and eastern suburbs [4]. In the 2010 Maule Earthquake, in Chile, the uplifting of the underground structures (manholes and tanks) were reported, and the underground tank in San Pedro del Valle was uplifted by approximately 1.2 m [5].

During a seismic event, loose saturated sands tend to decrease in volume, which produces an increase in the pore water pressures (P.W.P.), consequently a decrease in shear strength and reduction in effective stress. When the excess pore water pressures

(E.P.W.P.) reaches to a value equal to or more than the vertical effective stress, the soil is in a liquefied state [6-10]. The vertical effective stress below an underground shallow structure is generally small as it consists only from the weight of this light structure and the overburden pressure above. Thus the increase of the pore water pressures below of the structure would most probably lead to soil liquefaction as well as a floatation of this structure and getting out service [11-15]. In fact, it is necessary to properly design underground structures accounting for seismic loading and e liquefaction and uplift [16-19].

In this study, a 3D numerical model was devoted to the investigation of the performance of Hydro-Quebec underground structures under three different earthquakes (Table 1). The numerical modelling and material calibration as well as the model verification are introduced. Then the obtained results in term of both seismic soil and structure responses are presented. .

NUMERICAL MODEL

Physical model

Seismic behavior of access underground structure and liquefaction of the surrounding soil was investigated. The soil layer was assumed to be liquefied sand soil with 10m thickness overlay extended rock layer. The underground structure under consideration is a typical Hydro-Quebec chamber (4.0x2.0x3.0m) with two different diameter manholes (i.e., D = 0.6 and 1.0m) located at the upper slab and connected to the small sides with two square beams at the same level but not symmetric in position as shown in Fig. 1a. The structure and the two manholes are simulated by Liner Structural Elements while the two square beams are simulated by Beam Structural Elements. The spatial element size, Δl , must be smaller than approximately one-tenth of the wavelength of the input wave [20].

$$\Delta l \leq \frac{\lambda}{10} \quad (1)$$

Where λ is the wavelength associated with the highest frequency of the input earthquakes. Earthquakes used in this study have a max frequency of less than 20 Hz and the shear wave velocity of the soil is 150 m/s. therefore, the soil element size is chosen to be 0.5x0.5x0.5 m close to the structure and gradually increases whenever it goes outside as shown in Fig. 1b.

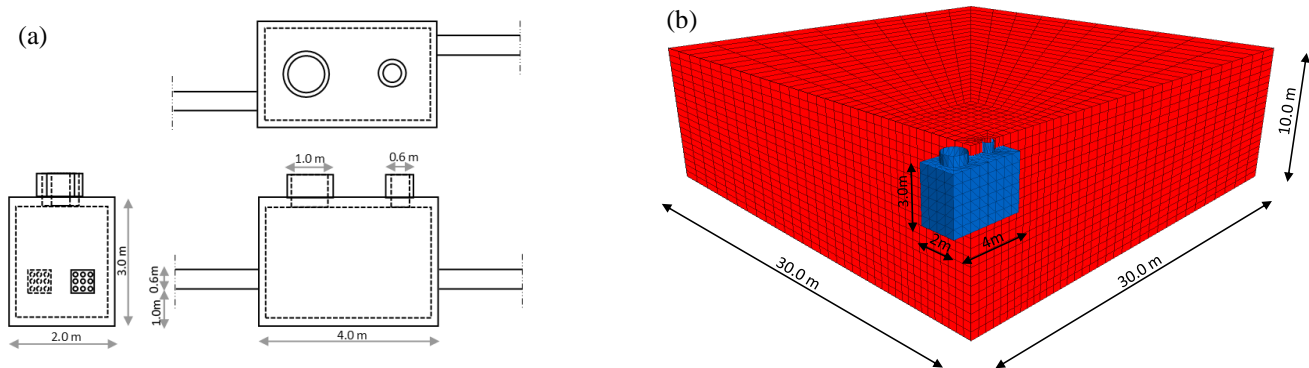


Figure 1. Numerical model: (a) Structure dimension, (b) Model layout.

Boundary conditions

Two types of boundary were chosen to simulate the model. First, the static analysis was used to compute gravity stresses, the base boundary was fixed both horizontally and vertically however the side boundaries were fixed only horizontally. Second, in the dynamic analysis, the horizontal seismic load was applied at the base boundary. The horizontal restraints of the side boundaries were released and replaced by the free field (FF) boundary condition. The groundwater level was assumed to be flat at the ground surface.

Material properties and damping

In this study, the soil layer was assumed to be loose saturated Ottawa sand with a 10 m thick overlying rigid rock. Its physical properties are described in Table 2. In the static analysis, the soils were represented by the Mohr-Coulomb model, while in situ stresses due to gravity were developed in the model. Sand parameters used in the numerical analyses (Table 3) were determined based on an assumed relative density (% $D_r=20$). During the dynamic stage, the displacements within the model were reset to zero. The sandy ground was modeled using the energy-based approach constitutive model. The structure was assumed to be elastic material with a Young modulus and Poisson ratio of 30 GPa and 0.2, respectively. Hysteretic damping (SIG4) was selected to produce shear modulus degradation and damping curves. Additionally, a Rayleigh damping ratio of 0.002 was used to ensure the stability of the numerical solution process at very low strain levels, as recommended by the FLAC software manual [20].

Material calibration and Model validation

During soil liquefaction, some of the motion shear energy is dissipated. Seed and his colleagues at the University of California at Berkeley developed an energy-based pore pressure generation model as an alternative to the well-known stress-based model [21]. The motivation for the development of this model was to enable them to use the dissipated energy as a measure of soil liquefaction resistance. The pore water pressure buildup is directly related to the amount of seismic energy dissipated in the unit volume of soil. The excess pore water pressure ratio (r_u) can be then estimated from the cyclic energy per unit volume of the soil [22-23]. More recent laboratory test results obtained from the strain-controlled triaxial simple shear TxSS apparatus by Karray et al., 2015[24] confirmed that the dissipated energy per unit volume during cyclic loading is closely connected to the generated excess pore water pressure. The relationship between dissipated energy and excess pore pressure ratio is:

$$r_u = \alpha \left(\frac{W_s}{\alpha_x} \right)^\beta \tag{2}$$

where W_s is the energy dissipated per unit volume of soil divided by the initial effective confining pressure, which is determined by integrating the area bound by stress-strain hysteresis loops, α , β , and α_x are parameters that depend on the soil being tested.

Before describing the results of the seismic analyses of underground structures, the liquefaction parameters α , β , and α_x were calibrated, the applicability of the adopted energy-based approach to study the soil behavior under cyclic loading has been carried out through the simulation of cyclic simple shear tests on a sand quarry at the Sile region of Istanbul and named as Sile Sand [25]. The physical properties of Sile sand are given also in Table 2, and the sand parameters used in the numerical simulation are listed in Table 3. These parameters were determined based on the known relative density of the soil ($Dr = 20\%$). In the analysis, shear stress is applied to the top of a soil element having a fixed base and free top as a sin wave with a 6 kPa amplitude and 0.1 Hz frequency. The results of the analysis are compared to the previous test results [26] in term of shear stress-strain path (Fig. 2a); excess pore water pressure ratio response (Fig. 2b). The comparative results presented in Figs. 2 indicate that the current energy-based model has the capability to reasonably simulate the cyclic behavior of sand. The applicability of the used soil constitutive model in particular and the adopted numerical model in general to the analysis of the seismic behavior of the underground structure is examined by the simulation of centrifuge experiments conducted on the seismic performance of a circular tunnel embedded in a uniform horizontal fully saturated sand [27]. From Figs. 3a and 3b, it can be found that the built up of excess pore water pressure ratios, r_u computed at the spring of the tunnel and tunnel uplift are very close to their measured counterparts. And therefore, it could be concluded that the numerical model adopted in the present investigation is capable of simulating the seismic behavior of underground structures.

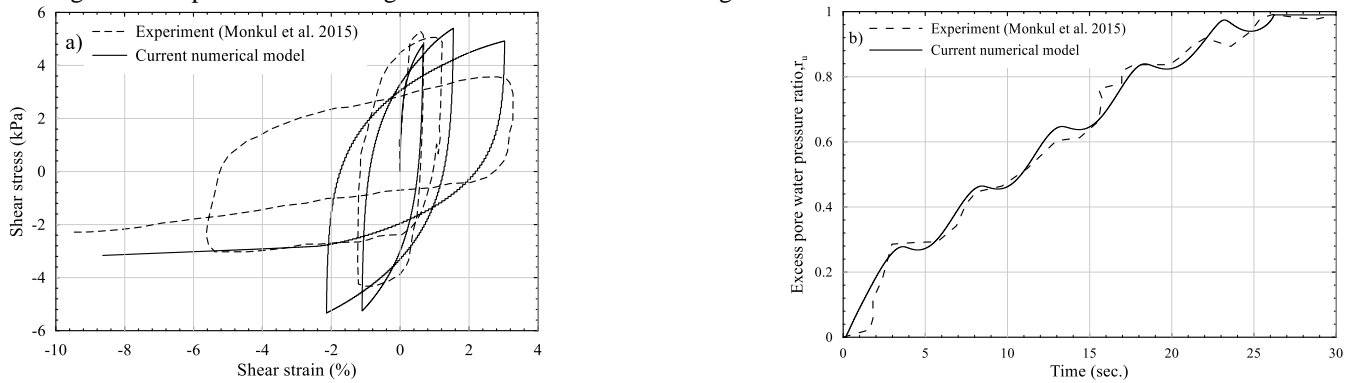


Fig. 2 Comparison between cyclic simple shear test results of Monkul et al. (2015) and current numerical simulations (a) shear stress-strain path (b) excess pore water pressure ratio r_u .

Table 1. Example of a Table.

Earthquake	Location	f (Hz)	Classification
Saguenay	Quebec (CA1988)	3.33	High
Loma Prieta	California (US1989)	1.56	Intermedia
Great Hanshin	Kobe (JP1995)	0.75	Low

Table 2: Physical properties of sands used in this study

Sand	Ottawa	Sile	Hoston
D_{50}	0.40	0.47	0.42
e_{max}	0.82	0.78	0.94
e_{min}	0.50	0.48	0.58

Table 3: Materials parameters used in the numerical simulation.

Parameters	G_0 (MPa)	K_0 (MPa)	ρ_d (kg/m ³)	k (m/s)	ϕ_f°	n	α	β	a_x	E_c (GPa)	ν_c
value	15	40	1500	1.00E-05	33	0.43	1	0.6	1.1	2.5	0.15

G_0 : initial shear modulus at a confining pressure of 100 kPa; K_0 : initial bulk modulus at a confining pressure of 100 kPa; ρ_d : dry density; k : soil permeability; ϕ_f° : failure angle of friction; n : porosity; α , β and a_x : liquefaction parameters; E_c : Young's modulus of concrete; ν_c : Poisson's ratio of concrete.

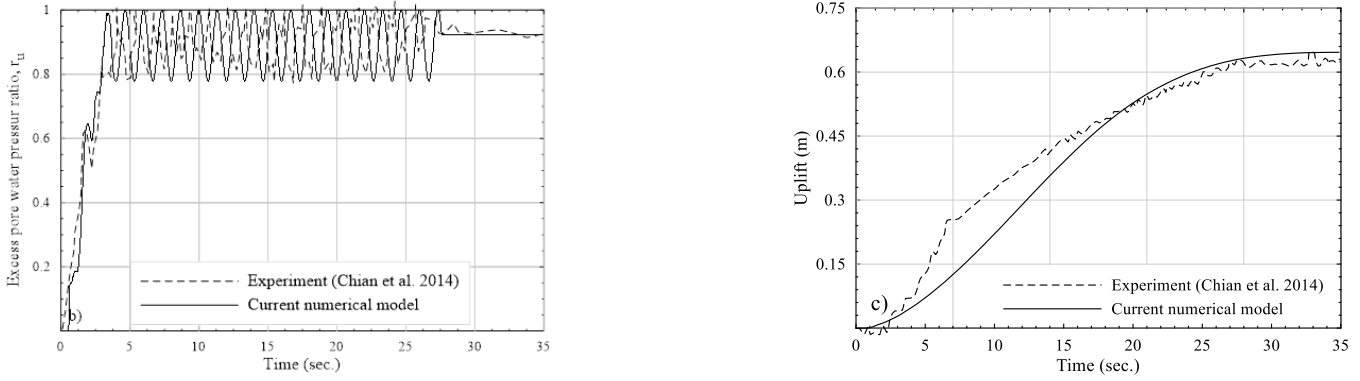


Fig. 3 Comparison between cyclic simple shear test results of simulations Chian et al. (2014) and current numerical model (a) measured and computed time histories of r_u at spring level (b) measured and computed time histories of structure uplift.

Input earthquakes

The frequency content of earthquakes can be the most important parameter to explain the damage occurred during strong earthquakes. The ground earthquakes recorded worldwide during recent decades show various frequency contents, from high and intermediate frequency earthquakes to low frequency earthquakes. Three earthquakes with different frequency were used as input motions in this study. These earthquakes are: I) Saguenay earthquake which is one of the largest recorded earthquakes in eastern North America during the last century; II) Loma Prieta earthquake which is one of the most powerful and destructive quakes ever to hit a populated area of the United States; III) Great Hanshin earthquake which led to Kobe destroyed. The PGA of the three earthquakes are scaled to 0.5, 1.0, 1.5 g to study the amplitude effect. The normalized acceleration time histories of the different earthquakes are shown in Figs. 4.

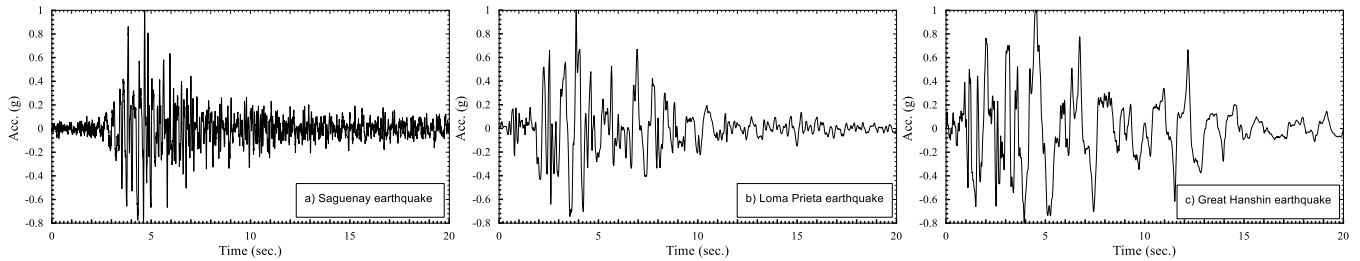


Fig.4 Input earthquakes time histories:(a) Saguenay earthquake; (b) Loma Prieta earthquake; (c) Great Hanshin earthquake.

NUMERICAL RESULTS

Liquefaction ratio

Figures 5 show the time histories of the excess pore water pressure ratio of the soil at the soil base and directly below the structure due to the change in the applied seismic motion. In Fig. 5a., it is can be seen that the PGA of Loma earthquake has a direct impact on the developed built up pore water pressure at the base of liquefied soil. As expected, the time of liquefaction occurrence decreases with the earthquake amplitude. Soil subjected to an earthquake with PGA=0.5g needs 6.6 sec to liquefy while that exposes to 1.5g earthquake needs only 2.8 sec to reach the same situation. While as it can be shown in Fig. 5b., the earthquake frequency content is more effective than the earthquake amplitude where Kobe earthquake ($f=0.75$ Hz) needs only 2.0 sec to liquefy the soil while Loma earthquake ($f=1.56$ Hz) liquefies the soil through 4 sec. However, Saguenay earthquake ($f=3.33$ Hz) could not reach r_u to 1. Comparing Figs. 5b. and 5c., it can be observed that the soil liquefaction under the structure is related to the soil liquefaction at the base. The increase in the excess pore water pressure under the structure stops approximately at the

same time of liquefaction occurs at the base in both Kobe and Loma Earthquakes (after 2 and 4 sec. respectively). While in Saguenay earthquake, where there is no liquefaction occurred at the base, the excess pore water pressure ratio under the structure continued to increase even after the earthquake has been ended. By the end of the three earthquakes, the excess pore water pressure under the structure is approximately the same ($R_u=0.8$) for the three earthquakes.

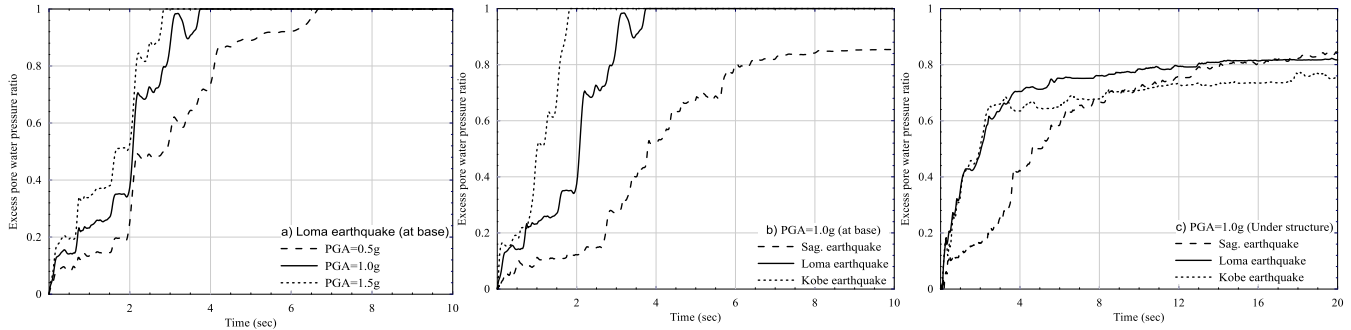


Fig. 5 Time history of liquefaction ratio: (a) at the soil base with different PGA (Loma Earthquake); (b) at the soil base with different earthquakes (PGA = 1.0g); (c) under the structure with different earthquakes (PGA = 1.0).

Ground motion response

Figures 6 show the effects of the earthquake parameters (amplitude and frequency) on the acceleration response at the ground surface. In Fig. 6a, where the PGA of the three earthquakes are normalized to be 1g, it is found that the decrease of the earthquake frequency has two main effects: (a) it decreases the natural frequency of the soil deposit due to the reduction of shear wave velocity (shear modulus) with acceleration amplitude (strain level); (b) it reduces the peak values because of the increase of soil damping with shear strain. The same thing can be clearly seen in Fig. 6b, with the increasing of earthquake amplitude, but it can be observed that the effect of the earthquake frequency multiplication is not less than the earthquake amplitude on the ground motion amplification. In Fig. 6c, Saguenay earthquake (PGA=1g) is applied to two soils: liquefied and not liquefied soils, and it can be seen that there are no significant difference between the two cases because there is no complete liquefaction has been occurred due to this particular earthquake as it was mentioned above.

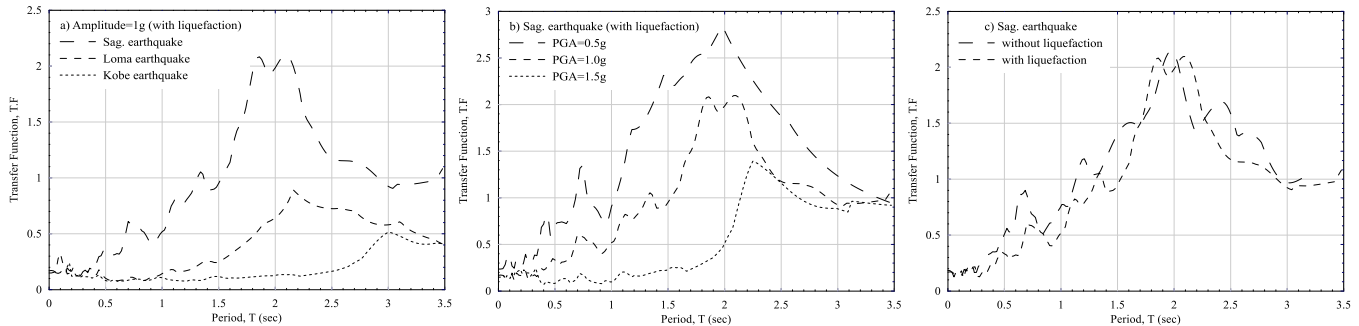


Fig. 6 Transfer Function between the output Fourier-Amplitude spectra at the surface to the input Fourier-Amplitude spectra at the base: (a) for different frequency contents; (b) for different earthquake amplitudes.

Internal forces

Figure 7 and 8 show the increase and the decrease in the dynamic bending moment due to seismic loads compare to the static moment of the selected elements considering the loading conditions of the three different earthquakes. In Fig. 7a, the dynamic bending moment of the long-side wall increases from about 40-55% to 115-155% due to increase the earthquake amplitude from 0.5g to 1.0g. However, reduction occurred in the bending moment when the earthquake amplitude reached a value of 1.5g. This reduction is the result of fast liquefaction that takes place in this case (3 sec.). While in Fig. 7b, despite the different intensity of the three earthquakes, the dynamic bending moment of the three earthquakes (same amplitude) increased with the same ratio 100-155% approximately. This is due to the fact that liquefaction occurs in the strong earthquake faster than the less severe quake and liquefaction tends to reduce the earthquake power and deamplifies the earthquake acceleration. Figure 7c explains the effect of liquefaction occurrence on the dynamic bending moment. It is found that the liquefaction leads to a reduction in the dynamic bending moment due to the associated reduction in the earthquake energy. On the other hand, there is a reduction in the dynamic bending moment of the based slab with the increase of the earthquake amplitude as shown in Fig. 8a. This reduction is, in fact, resulted from the reverse moment generated from the additional deformations and stresses in the side walls. Also, in Fig. 8b, there

is a reduction in the dynamic bending moment of the based slab with the three different earthquakes. Also, in Fig. 8c, it is can be seen that the reduction of base bending moment in case of liquefaction occurrence is more than the case free of liquefaction.

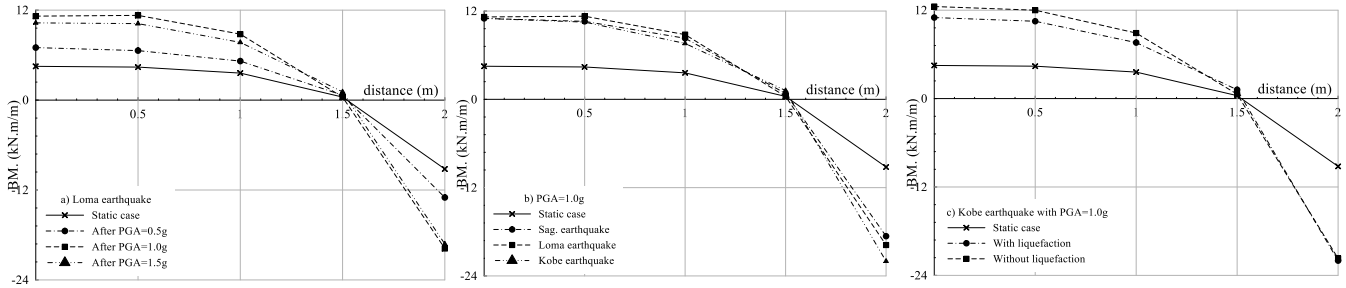


Fig. 7 Numerical result of the bending moment of the long side wall in the horizontal level (a) after Loma Prieta earthquake with different PGA; (b) after the three different earthquakes with 1g PGA; (c) after Great Hanshin earthquake with 1g PGA with and without liquefaction.

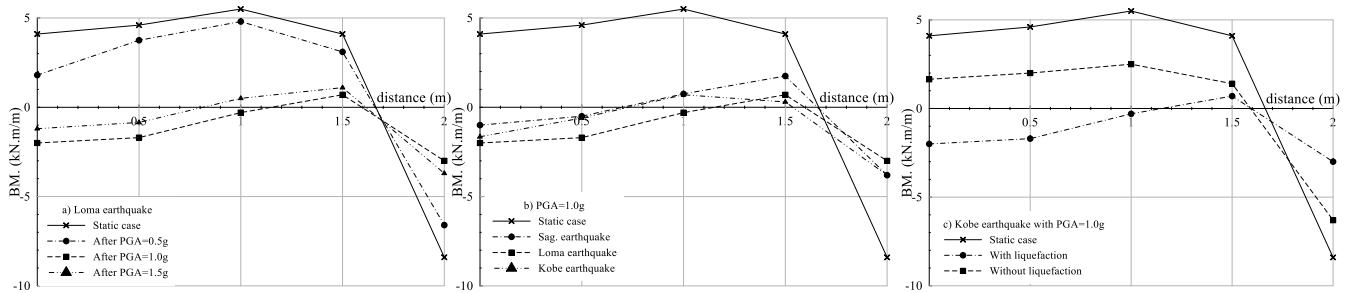


Fig. 8 Numerical result of the bending moment of the base slab in the long direction (a) after Loma Prieta earthquake with different PGA; (b) after the three different earthquakes with 1g PGA; (c) after Great Hanshin earthquake with 1g PGA with and without liquefaction.

The same trends have been observed in shear forces as shown in Fig. 9a, where the increase in the pressure of the soil surrounding the side walls of the structure leads to an increase of the shear forces in the both long- and short-side walls. The extra deformations and stresses in the side walls give rise to generate deformations and stress reverse the deformations resulting from the soil structure base slab interaction. While in Fig. 9b, despite the different intensity of the three earthquakes, the normalized shear forces in the both long- and short-side walls due to the three earthquakes (same amplitude) increased to approximately the double and the shear forces in the base slab reduce to the half. In Fig. 9c, where no liquefaction occurred, the increase of the frequency content leads to a reduction in the dynamic shear forces of the side walls and slab base.

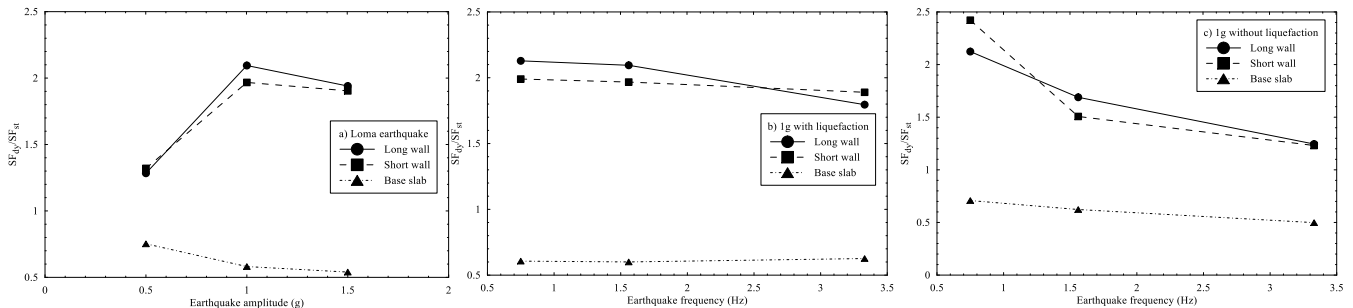


Fig. 9 Numerical result of the normalized shear force at different elements (a) after Loma Prieta earthquake with different PGA; (b) after the three different earthquakes with 1g PGA with liquefaction; (c) after the three different earthquakes with 1g PGA without liquefaction.

CONCLUSIONS

Three-dimensional numerical simulations were conducted in this paper to study the seismic performance of access underground structure to study the effects of the earthquake parameters (i.e., amplitude and frequency) and liquefaction occurring. The energy-based approach was used as a constitutive model to simulate the seismic behavior of the soil. The acceleration response, the excess pore pressure, and the internal forces of the underground structure (i.e., shear forces and bending moment) were investigated. From the numerical results, the following conclusions can be obtained:

1. When the liquefaction occurs the liquefaction works to quell the earthquake power and deamplification the earthquake acceleration.
2. Earthquake amplitude increasing also of earthquake frequency decreasing content lead to deamplification of the ground surface accelerations. However, multiple of the earthquake frequency content is more effective than multiple of the earthquake amplitude.
3. Increase and decrease in the dynamic internal forces of the side walls and slab base respectively by an increase of earthquake intensity. However, the liquefaction occurring works on reduction these changes.

ACKNOWLEDGMENTS

The authors would also like to thank Hydro-Québec and the Natural Sciences and Engineering Research Council of Canada (NSERC) for their financial support throughout this research project.

REFERENCES

- [1] Lecomte E., Pang A. and Russell J. (1998). La tempête de verglas de 1998, Document de recherche de l'IPSC.
- [2] Guérin, M., Mohamed H. and Benmokrane, B. (2016). Fatigue behaviour of concrete underground chambers reinforced with GFRP bars, CSCE annual conference, STR-824: 1-9.
- [3] Tokimatsua, K., Tamurab, S., Suzukia, H. and Katsumata K. (2012). Building damage associated with geotechnical problems in the 2011 Tohoku Pacific earthquake, *Soils and Foundations*, 52(5): 956-974.
- [4] Kaiser A., Holden C., Beavan J., Beetham D., Benites R., Celentano A., Collett D., Cousins J., Cubrinovski M., Dellow G., Denys P., Fielding E., Fry B., Gerstenberger M., Langridge R., Massey C., Motagh M., Pondard N., McVerry G., Ristau J., Stirling M., Thomas J., Uma SR. and Zhao J. (2012). The Mw 6.2 Christchurch earthquake of February 2011: preliminary report, *New Zealand Journal of Geology and Geophysics*, 55(1): 67:90.
- [5] Kang, G., Chung, J., and Iai, S. (2014). Seismic simulation of liquefaction-induced uplift behavior of a hollow cylinder structure buried in shallow ground, *Soil Dynamics and Earthquake Engineering*, 64: 85–94.
- [6] Zhou, J., Jiang, J. and Chen X. (2015). Micro-and macro-observations of liquefaction of saturated sand around buried structures in centrifuge shaking table tests, *Soil Dynamics and Earthquake Engineering*, 72: 1–11.
- [7] Rauch, A. F., (1997). An Empirical Method for Predicating Surface Displacements Due to Liquefaction-Induced Lateral Spreading in Earthquakes, A Thesis Submitted for the Degree of Doctor of Engineering, Virginia polytechnic institute and state university.
- [8] Youd, T. L., (1973). Liquefaction, Flow, and Associated Ground Failure, U.S. geological survey circular, 688:1-12.
- [9] Kramer, S. L. and Elgamal A. W., (2001). Modeling Soil Liquefaction Hazards for Performance-Based Earthquake Engineering, PEER Report 2001/13, University of California, California, USA.
- [10] Slade, J. A., Hollande, R. D. and Kraha. J., (1985). The liquefaction of sands, a collapse surface approach, *Canadian Geotechnical Journal*, 22: 564-578.
- [11] Koseki, J., Matsuo, O., Ninomiya, Y. and Yoshida, T. (1997). Uplift of sewer manhole during the 1993 Kushiro-Oki earthquake, *Soils and Foundations*, 37(1): 109-121.
- [12] Kutter, M., Chou, S. and Travasarou, A. (2008). Centrifuge Testing of the Seismic Performance of a Submerged Cut-and-Cover Tunnel in Liquefiable Soil, *Geotechnical Earthquake Engineering and Soil Dynamics IV*, DOI: 10.1061/40975(318)204.
- [13] Tobita, T., Kang, G. and Iai, S. (2011). Centrifuge modeling on manhole uplift in a liquefied trench, *Soils and Foundations*, 51(6):1091-1102.
- [14] Wang, Z., Lu, Y., Hao, H. and Chong K. (2005). A full coupled numerical analysis approach for buried structures subjected to subsurface blast, *Computers and Structures*, 83: 339–356.
- [15] Zhou, J., Jiang, J. and Chen X. (2015). Micro-and macro-observations of liquefaction of saturated sand around buried structures in centrifuge shaking table tests, *Soil Dynamics and Earthquake Engineering*, 72: 1–11.
- [16] Liu, H. and Song, E. (2005). Seismic response of large underground structures in liquefiable soils subjected to horizontal and vertical earthquake excitations, *Computers and Geotechnic*, 32: 223–244.
- [17] Orense, R., Morimoto, I., Yamamoto, Y., Yumiyama, T., Yamamoto, H. and Sugawara, K. (2003). Study on wall-type gravel drains as liquefaction countermeasure for underground structures, *Soil Dynamics and Earthquake Engineering*, 23: 19–39.
- [18] Kang, G., Tobita, T., Iai, S., and Ge, L. (2013). Centrifuge Modeling and Mitigation of Manhole Uplift due to Liquefaction, *Journal of Geotechnical and Geoenvironmental Engineering*, 39:458-469.
- [19] Ling, H., Mohri, Y., Kawabata, Y., Liu, H., Burke, C., and Sun, L. (2003). Centrifugal Modeling of Seismic Behavior of Large-Diameter Pipe in Liquefiable Soil, *Journal of Geotechnical and Geoenvironmental Engineering*, 129:1092-1101.
- [20] Itasca Consulting Group. (2013). FLAC3D: Fast lagrangian analysis of continua in 3-dimensions 5.01, manual. Itasca, Minneapolis.

- [21] Booker, J.R., Rahman, M.S. & Seed, H.B. (1976). GADFLEA – A Computer Program for the Analysis of Pore Pressure Generation and Dissipation During Cyclic or Earthquake Loading. EERC 76-24. University of California, Berkeley.
- [22] Davis, R.O., and Berrill, J.B. (1982). Energy dissipation and seismic liquefaction in sands. *Earthquake Engineering & Structural Dynamics*, 10(1): 59–68.
- [23] Berrill, J.B., and Davis, R.O. (1985). Energy dissipation and seismic liquefaction of sands: revised model. *Soils and Foundations*, 25(2): 106–118.
- [24] Karray, M., Hussien, M. and Chekired M. (2015). Evaluation of compatibility between existing liquefaction charts in Eastern regions of North America. The 68th Canadian Geotechnical Conference, Québec, Canada.
- [25] Eseller-Bayat, E., Monkul, M., Akin, Ö. and Yenigun, S. (2017). The Coupled Influence of Relative Density, CSR, Plasticity and Content of Fines on Cyclic Liquefaction Resistance of Sands, *Journal of Earthquake Engineering*.
- [26] Monkul, M., Gültekin, C., Gülver, Ö., Akin, T. and Eseller-Bayat, E. (2015). Estimation of liquefaction potential from dry and saturated sandy soils under drained constant volume cyclic simple shear loading, *Soil Dynamics and Earthquake Engineering*, 75: 27–36.
- [27] Chian, S.C., Tokimatsu, K. and Madabhushi, S. P. G. (2014). Soil liquefaction–induced uplift of underground structures: physical and numerical modeling, *Journal of Geotechnical and Geoenvironmental Engineering*, 140(10): 04014057.